December 2004 • NREL/CP-500-36756

Conference Paper

Stability Analysis of an Adaptive Torque Controller for Variable Speed Wind Turbines

Preprint

K.E. Johnson, L.Y. Pao, M.J. Balas, V. Kulkarni, and L.J. Fingersh

To be presented at the IEEE Conference on Decision and Control
Paradise Island, Bahamas
December 14–17, 2004

National Renewable Energy Laboratory
1617 Cole Boulevard, Golden, Colorado 80401-3393
303-275-3000 • www.nrel.gov

Operated for the U.S. Department of Energy
Office of Energy Efficiency and Renewable Energy
by Midwest Research Institute • Battelle

Contract No. DE-AC36-99-GO10337

NOTICE

Available electronically at http://www.osti.gov/bridge

Available for a processing fee to U.S. Department of Energy and its contractors, in paper, from:

U.S. Department of Energy
Office of Scientific and Technical Information
P.O. Box 62
Oak Ridge, TN 37831-0062
phone: 865.576.8401
fax: 865.576.5728
email: mailto:reports@adonis.osti.gov

Available for sale to the public, in paper, from:

U.S. Department of Commerce
National Technical Information Service
5285 Port Royal Road
Springfield, VA 22161
phone: 800.553.6847
fax: 703.605.6900
email: orders@ntis.fedworld.gov
online ordering: http://www.ntis.gov/ordering.htm

Printed on paper containing at least 50% wastepaper, including 20% postconsumer waste

Stability Analysis of an Adaptive Torque Controller for Variable Speed Wind Turbines

Kathryn E. Johnson, Lucy Y. Pao, Mark J. Balas, Vishwesh Kulkarni, and Lee J. Fingersh

***Abstract*—Variable speed wind turbines are designed to follow wind speed variations in low winds in order to maximize aerodynamic efficiency. Unfortunately, uncertainty in the aerodynamic parameters may lead to sub-optimal power capture in variable speed turbines. Adaptive generator torque control is one method of eliminating this sub-optimality; however, before adaptive control can become widely used in the wind industry, it must be proven to be safe. This paper analyzes the stability of an adaptive torque control law and the gain adaptation law in use on the Controls Advanced Research Turbine (CART) at the National Renewable Energy Laboratory's National Wind Technology Center.**

I. INTRODUCTION

THERE are many different types of wind turbines in use around the world, each having its own list of benefits and drawbacks [1]. Modern horizontal axis wind turbines (HAWTs) typically have two or three blades and can be either upwind (with the rotor spinning on the upwind side of the tower) or downwind. In order for a variable speed turbine to achieve its maximum power capture, complex aerodynamic properties must be well known; in practice, these uncertainties can easily lead to a variable speed turbine capturing less power than is possible. Adaptive control can solve this problem, and the research presented in this paper addresses the stability of a recently proposed adaptive control approach [2].

Many utility-scale turbines have two fast active control systems. The first is generator torque control, which opposes the aerodynamic torque provided by the wind and thus controls turbine speed. The second is active pitch control, wherein either the entire blade or some section thereof can be rotated on demand. This paper focuses on adaptive generator torque control (for a constant blade pitch) to maximize energy capture in region 2 of a variable speed wind turbine.

Variable speed wind turbines have three main regions of operation. The first, region 1, includes the time when the turbine is starting up. Region 2 is an operational mode in which it is desirable to capture as much power as possible from the wind. Region 3 is encountered when the wind speeds are high enough that the turbine must limit the fraction of the wind power captured so that safe electrical and mechanical loads are not exceeded. Fig. 1 gives an example of the desired power vs. wind speed for a variable speed wind turbine with a 43.3 meter rotor diameter and shows the three major control regions.

In Fig. 1, the power coefficient, C_p, is defined as the ratio of the rotor power to the power available in the wind, P_{wind}:

$$C_p = \frac{P}{P_{wind}} \tag{1}$$

where

$$P_{wind} = \tfrac{1}{2}\rho A v^3 . \tag{2}$$

In (2), ρ is the air density, A is the rotor swept area, and v is the wind speed. The power P in (1) can be defined in different ways, which can result in slightly different interpretations of C_p; however, the most common definition

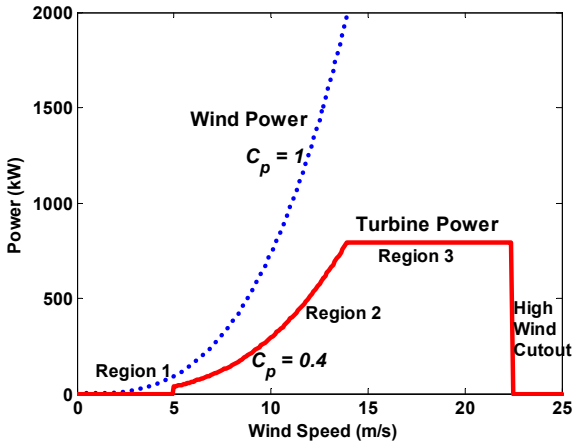

Fig. 1. Steady-state power curves for wind and example turbine. Note that a real turbine must limit power to a certain maximum load.

This work was supported in part by the U. S. Department of Energy (through the National Renewable Energy Laboratory under contract number DE-AC36-99G010337), the University of Colorado at Boulder, and the American Society for Engineering Education.

K. E. Johnson is with the National Renewable Energy Laboratory, Golden, CO, 80401 USA (phone: 303-384-6916; fax: 303-384-6901; email: kathryn.e.johnson@colorado.edu).

L. Y. Pao is with the Electrical Engineering Department, University of Colorado, Boulder, CO 80309 USA (pao@colorado.edu).

M. J. Balas is with the Electrical Engineering Department, University of Wyoming, Laramie, WY 82071 USA (mbalas@uwyo.edu).

V. Kulkarni is with the Electrical Engineering Department, University of Colorado, Boulder, CO 80309 US (Vishwesh.Kulkarni@colorado.edu).

L. J. Fingersh is with the National Renewable Energy Laboratory, Golden, CO, 80401 USA (email: lee_fingersh@nrel.gov).

considers P to be the aerodynamic rotor power:

$$P = \tau_{aero}\omega \tag{3}$$

where τ_{aero} is the aerodynamic torque applied to the rotor by the wind and ω is the rotor angular speed. In Fig. 1, the dotted "Wind Power" curve represents the power of the unimpeded wind passing through the rotor swept area. The solid curve represents the power that could be extracted by an example real turbine. Given the dynamics of the wind and turbine, there is not a one-to-one correlation between wind speed and turbine power, but the "Turbine Power" curve plotted in Fig. 1 represents the desired steady-state relationship for the example turbine.

Classical techniques such as PID control of blade pitch [4] are typically used to limit power and speed for turbines operating in region 3, and some type of generator torque control [5] is used in region 2. Although the specific techniques used to control modern turbines are proprietary and typically unpublished, it is believed that only very recently have turbine manufacturers begun to incorporate more modern and advanced control methods in commercial turbines. In part, this gap between the research and commercial turbine communities is a result of the fact that so few theoretically-based controllers have been successfully tested on real turbines.

The research presented here provides a stability analysis for a system that has already been tested on a real turbine. In past work, we developed a very intuitive adaptive strategy along with other techniques for improving wind turbine performance [2], [3]. This paper now analyzes the stability of the adaptive torque control. We begin with an introduction to the standard non-adaptive controller, continue with a discussion of the recently proposed adaptive controller, and then proceed to the stability analysis.

II. STANDARD VARIABLE SPEED CONTROL LAW

The standard control law for variable speed wind turbines in region 2 is intended to maximize energy capture by causing the turbine to operate at the peak of its C_p-TSR-Pitch surface. From (1), we see that rotor power P increases with C_p, so operation at $C_{p_{max}}$ is clearly desirable. As shown in Fig. 2, C_p is a function of blade pitch and tip speed ratio λ, where

$$\lambda = \frac{\omega R}{v}. \tag{4}$$

A standard control law that has commonly been used for region 2 control of variable speed turbines is to set the control torque τ_c (i.e., generator torque) equal to a gain K times the rotor speed squared:

$$\tau_c = K\omega^2 \tag{5}$$

where

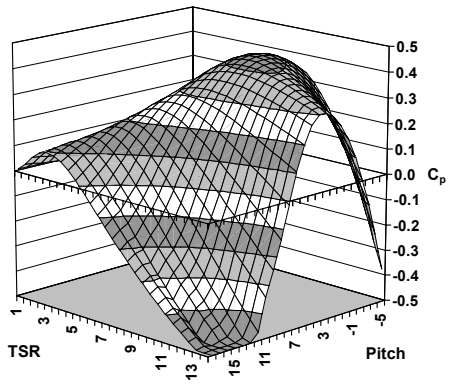

Fig. 2. C_p vs. TSR and Pitch for the CART. Turbine power is proportional to C_p, so it is desirable for the turbine to operate at the peak of the surface.

$$K = \frac{1}{2}\rho A R^3 \frac{C_{p_{\max}}}{\lambda_*^3}. \tag{6}$$

R is the rotor radius, $C_{p_{max}}$ is the maximum power coefficient, and λ_* is the tip speed ratio at which $C_{p_{max}}$ occurs. More details on the accurately modeled turbine's operation under the standard control (5) is provided in [2].

Fig. 2 was created with the modeling software PROP [6], which uses blade element momentum theory [7]. The PROP simulation was performed in order to obtain the operating parameters for the 600 kW Controls Advanced Research Turbine (CART). This two-bladed, upwind turbine at the National Renewable Energy Laboratory is the turbine test bed used in this research. Unfortunately, modeling tools such as PROP are not perfectly accurate, and fixed controllers designed using these modeling tools are generally still sub-optimal.

Even if the initially chosen gain K was optimal, wind turbine blades change over time due to problems like debris build-up and blade erosion, with the same net result as a sub-optimally chosen initial K. One study [5] shows how sensitive energy loss is to errors in λ_* and $C_{p_{max}}$. The study concludes that a very common 5% error in the optimal tip speed ratio λ_* alone can cause an energy loss of 1-3% in region 2, which is a significant loss in this industry.

III. ADAPTIVE CONTROL

A. Gain Adaptation Algorithm

In region 2, the adaptive control is very similar to the non-adaptive case presented in equations (5) and (6):

$$\tau_c = \begin{cases} 0, & \omega < 0 \\ \rho M \omega^2, & \omega \geq 0 \end{cases}. \tag{7}$$

The adaptive gain M incorporates all of the terms in the non-adaptive torque control gain K except the air density ρ, which is kept separate because it is uncontrollable. M is adapted after a certain number n time steps of operation in region 2; n is selected to be large enough to average out high frequency wind variations and the slowness of the

turbine response. Testing on the CART indicates that the adaptation period will need to be on the order of hours. This long time period is required in part because of the difficulty involved in obtaining a high correlation between measurements of wind speed at the rotor and at the meteorological tower. Another reason is that the turbine changes speed at a much slower rate than the wind and the slow responses must be averaged out over time. This long adaptation period should not cause significant problems for a commercial turbine designer because it is still very short compared to the decades-long life of a turbine.

The control law (7) is split between positive and negative regions of ω because it is not desirable to apply torque control when the turbine is spinning in reverse. Most turbines have separate control mechanisms to prevent reverse operation, and, except where specifically noted, this research assumes positive operation only.

We conducted a simulation using a rigid body model relating net torque and angular acceleration as

$$\dot{\omega} = \tfrac{1}{J}\left(\tau_{aero} - \tau_c\right), \tag{8}$$

where J is the rotational inertia, and using (7) for the control torque. This simulation was run for 200 seconds with each of 26 different values of the gain M, and the turbine's behavior for each of the 26 gain values was averaged over the 200 seconds in order to produce the solid "P_{favg}" curve in Fig. 3. In Fig. 3, $M^* = 174.5$ is the assumed optimal gain based on the standard torque control coefficient K in (6) and the simulated C_p surface in Fig. 2. $\tilde{M}$ is the error in M:

$$\tilde{M} = M^* - M\,. \tag{9}$$

P_{favg}, computed in discrete time at a rate of f_s/n, is the ratio of the mean power captured to the mean wind power (both of which are continuous time signals sampled at f_s = 100 Hz on the CART) and is computed as:

$$P_{favg}(k) = \frac{\frac{1}{n}\sum_{i=1}^{n} P_{cap}(k-n+i)}{\frac{1}{n}\sum_{i=1}^{n} P_{wy}(k-n+i)} \tag{10}$$

where P_{wy} is the wind power including yaw error, given by

$$P_{wy} = \tfrac{1}{2}\rho A v^3 \cos^3(\psi), \tag{11}$$

and P_{cap} is the captured power, given by

$$P_{cap} = \tau_c \omega + J\omega\dot{\omega}\,. \tag{12}$$

The yaw error factor ($\cos^3(\psi)$) in (11) is a necessary component of the available power calculation that is discussed further in [3]. The first term in P_{cap} is the generator power and the second is the kinetic power (i.e., the time derivative of the kinetic energy) of the rotor. The reason that P_{cap} is used in (10) rather than the turbine power P given by (3) is that the sensor requirements are better suited to the instrumentation normally available on an industrial turbine. The two definitions of the turbine's power are closely related, differing only by the mechanical losses in the turbine's gearbox that make $P_{cap} < P$ by a small amount. Given that fact and also $P_{wind} \geq P_{wy}$, it is impossible to state whether $P_{favg} < C_p$ as defined in (1) or vice versa at any given instant. However, the magnitude of P_{favg} doesn't matter as long as $M \rightarrow M^*$.

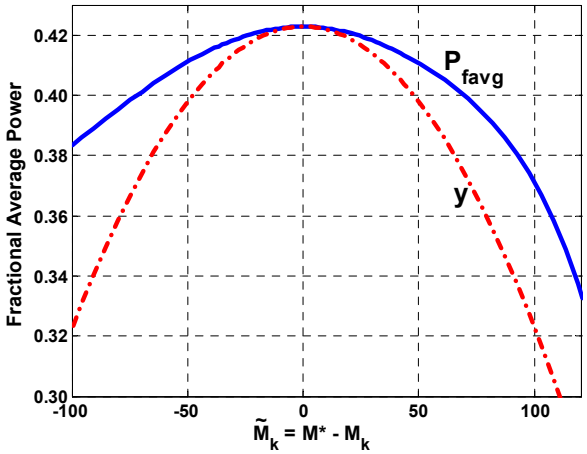

Fig. 3. Ratio of mean captured power to mean wind power vs. error in torque control gain M. The gain adaptation law uses some properties of the P_{favg} curve, including the finite maximum and the monotonic nature on either side of the maximum. The y curve is used in section IV.D.3.

The controller begins by changing M by some ΔM. At the end of the adaptation period, the controller evaluates the turbine's performance. If the fraction of the average power P_{favg} is greater than the fractional mean power in the preceding adaptation period, the controller selects a new ΔM of the same sign as the previous one. This process continues in the same manner until the fractional power is less than that of the preceding adaptation period. At that point, the new ΔM is calculated to have the opposite sign of the previous ΔM. Eventually, M should converge toward M^*, the optimal gain.

The equations for this gain adaptation are

$$M(k) = M(k-n) + \Delta M(k) \tag{13}$$

$$\Delta M(k) = \gamma_{\Delta M}\,\mathrm{sgn}\left[\Delta M(k-n)\right]\mathrm{sgn}\left[\Delta P_{favg}(k)\right]\,\left|\Delta P_{favg}(k)\right|^{1/2} \tag{14}$$

$$\Delta P_{favg}(k) = P_{favg}(k) - P_{favg}(k-n)\,. \tag{15}$$

In (14), the $|\Delta P_{favg}(k)|^{½}$ factor is an indicator of the closeness of M to M^*. When M is such that operation is near the peak of the curve shown in Fig. 3, a given ΔM will cause a smaller $|\Delta P_{favg}|$ due to the flatter nature of the curve near its peak. Thus, $|\Delta M|$ decreases as the optimal gain is approached. The exponent ½ and the positive gain $\gamma_{\Delta M}$ are chosen based on empirical results in simulation. Selection of $\gamma_{\Delta M}$ will be addressed further in Section IV.D.

In this research, the controller attempts to have the turbine power track the wind power but assumes $C_{p_{max}}$ and λ_* are unknown. In contrast, previous adaptive controllers such as those in [8]-[9] focused on different uncertainties

and assumed some knowledge of the C_p surface, particularly λ_* and $C_{p_{max}}$. An additional difference among the various adaptive controllers is the lengthy averaging period used in this research, compared to the very short time periods used in previous adaptive controllers like [10].

Numerous simulations have been run to demonstrate that the adaptive controller (7) yields desired turbine behavior. These simulations, presented in [2], have used the characteristics of the CART and have demonstrated that the gain adaptation law given by (13) – (15) causes M to adapt towards the optimal gain and then oscillate around it. The amplitude of these oscillations is small (around 5% of M^*).

IV. STABILITY

We now address several stability questions that will help to ensure safe and desired operation of the adaptive torque gain control law. The first three questions relate to the stability properties of the torque control law—a continuous time problem on a rapid time scale. First, the simple problem of the asymptotic stability of the rotor speed to its equilibrium point in the absence of wind and in constant wind is addressed. Next, we show that a bounded input (i.e., wind) to the system produces a bounded output (rotor speed ω). Each of these stability results are shown under the assumption that the adaptive control gain $M > 0$ is constant; this is a valid assumption because the gain adaptation takes place discretely and on a time scale several orders of magnitude slower than that of the wind and rotor speed (many hours vs. seconds). The simplified block diagram for this system is given in Fig. 4(a), where the linear plant is (8) and the nonlinear controller is (7).

The final stability question regards the convergence of the adaptive gain $M \rightarrow M^*$ given the proposed gain adaptation law. Fig. 4(b) shows the simplified block diagram for this system, where the nonlinear plant is the P_{favg} vs. $\tilde{M}$ relationship shown in Fig. 3 and the nonlinear controller is given by (13) – (15). In all of these proofs the air density, ρ, is assumed to be a constant greater than zero. In reality, the changes in air density are small.

A. Asymptotic Stability of $\omega = 0$

Because wind turbines are designed to spin as freely as possible, the friction due to mechanical bearings and air resistance during operation is very small. However, in the formal proof of the asymptotic stability of the equilibrium point $\omega = 0$, we amend the equation for $\dot{\omega}$ in (8) to include a frictional term b, where $b > 0$:

$$\dot{\omega} = \tfrac{1}{J}\left(\tau_{aero} - \tau_c - b\omega\right). \tag{16}$$

The equation for aerodynamic torque, which is derived from (3), is

$$\tau_{aero} = \tfrac{1}{2}\rho A R C_q(\lambda,\beta)v^2, \tag{17}$$

where the torque coefficient C_q is given by

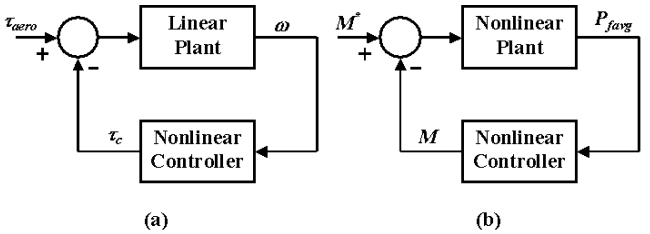

Fig. 4. Simplified block diagrams (a) relating aerodynamic torque and rotor speed, and (b) gain adaptation law. The continuous time diagram (a) is the topic of Theorems 1 and 2 and the discrete time diagram (b) is the topic of Section IV.D.

$$C_q(\lambda,\beta) = \frac{C_p(\lambda,\beta)}{\lambda}. \tag{18}$$

Given (17) and (7), (16) can be expanded to

$$\dot{\omega} = \begin{cases} \frac{1}{2J}\rho A R C_q v^2 - \frac{b}{J}\omega, & \omega < 0 \\ \frac{1}{2J}\rho A R C_q v^2 - \frac{\rho}{J}M\omega^2 - \frac{b}{J}\omega, & \omega \geq 0 \end{cases}. \tag{19}$$

Theorem 1: The plant (16) and the nonlinear controller (7) have an asymptotically stable equilibrium point at $\omega = 0$ when $v = 0$.

Proof: When $v = 0$, the first term in (19) becomes zero. In this case, the simple Lyapunov function candidate $V = \frac{1}{2}\omega^2$ has the derivative

$$\dot{V} = \begin{cases} -\frac{b}{J}\omega^2, & \omega < 0 \\ -\frac{\rho}{J}M\omega^3 - \frac{b}{J}\omega^2, & \omega \geq 0 \end{cases},$$

which is negative for $\omega \neq 0$ and is zero for $\omega = 0$. Thus, $\omega = 0$ is globally asymptotically stable equilibrium point.

We should also note that, when b is assumed to be zero, the equilibrium point is still stable in a global sense but no longer asymptotically stable for $\omega < 0$. The asymptotic stability still holds in a local sense for all $\omega \geq 0$.

B. Asymptotic Stability of Rotor Speed with Constant, Positive Wind Input

The next stability result to be addressed concerns whether or not the rotor speed ω converges to an equilibrium value under a constant, positive wind speed input. Although it is unreasonable to assume a constant wind speed in the field, it is still desirable to understand the system response under these controlled conditions. Once again, the plant is given by (16) and the nonlinear controller is given by (7). The adaptive controller (7) does not assume perfect knowledge of the aerodynamic parameters $C_{p_{max}}$ and λ_*. The cubic relationship between C_p and λ can be derived by setting the $\omega \geq 0$ part of (19) equal to zero:

$$C_p = \frac{\rho M \lambda^3 v + \lambda^2 b R}{\frac{1}{2}\rho A R^3 v} = G(\lambda, M, b, v). \tag{20}$$

In (20), b is several orders of magnitude smaller than M^*, so if it is assumed that M is within a neighborhood (say, an order of magnitude) of its true optimal value, the second term in the numerator of (20) is insignificant compared to

the first term in the numerator. Although this fact is not required for the following analysis, it simplifies the drawing of Fig. 5 because the wind speed v and air density ρ both cancel out and Fig. 5 can be drawn for various M values independently of v and ρ. When Fig. 5 is plotted using representative values of ρ, v, and b, its qualitative nature does not change, and the new curves are indistinguishable from those plotted on the scale in use.

Note in Fig. 5 that the cubic function does not intersect the CART's C_p curve at its peak when $M \neq M^*$. This is because optimal power capture cannot be achieved for $M \neq M^*$. Let λ_2 be defined as the tip speed ratio at the intersection of $G(\lambda,M)$ with the CART's C_p vs. λ curve, $C_p(\lambda)$, such that $G(\lambda,M) > C_p(\lambda)$ for all $\lambda > \lambda_2$., i.e., the highest value of λ for which the two curves intersect. Let λ_1 be defined as the next highest intersection point, i.e., the λ for which $0 < \lambda_1 < \lambda_2$ and $G(\lambda,M) < C_p(\lambda)$ for all $\lambda_1 < \lambda < \lambda_2$ and $G(\lambda,M) > C_p(\lambda)$ for some $\lambda < \lambda_1$ within a neighborhood of λ_1. For the dashed $M = 0.7M^*$ curve, these values correspond to $\lambda_1 = 3.1$ and $\lambda_2 = 8.4$. The following theorem states that, for a constant wind input, the tip speed ratio λ will converge to λ_2 as long as the initial λ is greater than λ_1. Assume $\lambda_1 > 0$.

Theorem 2: The plant (16) and the nonlinear controller (7) have a locally asymptotically stable equilibrium point at $\lambda = \lambda_2$ when v and M are constants greater than zero. The domain of attraction is $\lambda_1 < \lambda < \infty$.

Proof: In the domain $0 < \lambda_1 < \lambda < \infty$, $\omega > 0$ holds (since $\omega = \lambda v/R$). Define $\tilde{\lambda} = \lambda_2 - \lambda$. Now choose the Lyapunov function $V = \frac{1}{2}\tilde{\lambda}^2$. For $\omega > 0$,

$$\dot{V} = (\lambda - \lambda_2)\left(\tfrac{1}{2J}\rho AR^2 C_q v - \tfrac{1}{JR}\rho M\lambda^2 v - \tfrac{b}{J}\lambda\right). \qquad (21)$$

Substitution of C_p/λ for C_q in (21) and a little algebra provides the result that $\left(\tfrac{1}{2J}\rho AR^2 C_q v - \tfrac{1}{JR}\rho M\lambda^2 v - \tfrac{b}{J}\lambda\right) > 0$ when $\lambda_1 < \lambda < \lambda_2$ (i.e., when $G(\lambda,M) < C_p(\lambda)$). Also, $\left(\tfrac{1}{2J}\rho AR^2 C_q v - \tfrac{1}{JR}\rho M\lambda^2 v - \tfrac{b}{J}\lambda\right) < 0$ when $\lambda > \lambda_2$ because $\lambda > \lambda_2$ results in $G(\lambda,M) > C_p(\lambda)$ by definition of λ_2. Thus, $\dot{V} < 0$ for all $\lambda_1 < \lambda < \infty$ except $\lambda = \lambda_2$, for which $\dot{V} = 0$. This provides the result that the equilibrium point $\lambda = \lambda_2$ is locally asymptotically stable in the domain $\lambda_1 < \lambda < \infty$.

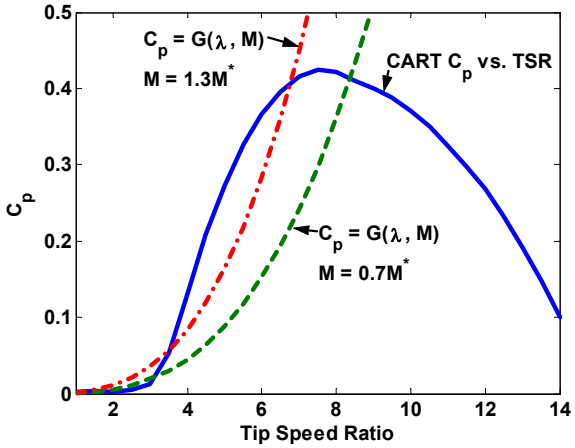

Fig. 5. CART C_p and cubic for different values of M

Note that this proof of the convergence of λ to a specific value is equivalent to the convergence of ω to a specific value for a specific wind speed because $\omega = \lambda v/R$. Also, note that when $M = M^*$, the curves $G(\lambda,M)$ and $C_p(\lambda)$ intersect at $(\lambda_*, C_{p_{max}})$ and therefore optimal power capture is achieved for the constant wind input case.

C. Input - Output Stability

All wind turbines have a maximum safe operating speed, and usually some type of aerodynamic braking is used to prevent the turbine from operating at speeds above this maximum. However, it is still useful to examine whether the torque control would bound the turbine speed in some sense in the absence of these other controllers. The proof for Theorem 3, which uses a passivity argument [11] has been omitted. More details can be found in [3].

Theorem 3: If $C_q \leq 1$, the plant (16) and the nonlinear controller (7) is $\mathcal{L}_2$ stable, where squared wind speed v^2 is the input and rotor speed ω is the output.

The condition $C_q \leq 1$ is nearly always satisfied for modern turbines. Indeed, since the Betz Limit (see, e.g., [7]) states that the maximum C_p for any real turbine is $^{16}/_{27}$, and the two curves are related by (18), we can guarantee that $C_q \leq 1$ for $\lambda \geq {}^{16}/_{27}$. When $\lambda \leq {}^{16}/_{27}$, the question is simple, since by the definition of λ in (4) it is known that $\omega = \frac{\lambda v}{R} \leq \frac{16}{27}\frac{v}{R}$. Thus, for finite λ, $\mathcal{L}_\infty$ stability is given.

Unfortunately, over an infinite horizon, v does not lie in $\mathcal{L}_2$. However, Theorem 3 provides a theoretical assurance over any finite lifetime of a turbine.

D. Convergence of the Gain Adaptation Algorithm

Since the gain adaptation law performs no calculations during $(k-n)T_s < t < kT_s$, M_{k-1} can replace M_{k-n} without loss of generality. (The discrete time index k has been changed to a subscript for convenience.) A few assumptions are made:

Assumption 1: M^* is constant. Although the turbine parameters (and thus the optimal gain M^*) change with time, this is a valid simplification because the turbine's physical changes are typically noticeable only over months or years, whereas the gain adaptation law has an adaptation period of less than a day.

Assumption 2: The P_{favg} vs. $\tilde{M}$ curve has a shape similar to the one in Fig. 3, at least in some local region around the optimal operating point. This is generally assumed to be true for any modern turbine. Specifically, the curve has a maximum at $\tilde{M} = 0$, is continuously differentiable, and is

strictly monotonically increasing on $\tilde{M} < 0$ and strictly monotonically decreasing on $\tilde{M} > 0$.

Assumption 3: The adaptive controller has been operating sufficiently long that the specifics of the initial conditions provided to the controller are no longer relevant. If the initial conditions provided are M_0, P_{favg_0}, ΔM_0, and M_1, then $k > 2$ is the time frame of interest.

1. Types of Instability

We begin by considering the possible ways that the system could go unstable (i.e., $|\tilde{M}| \to \infty$ as $k \to \infty$). One possibility is for $|\tilde{M}_k| > |\tilde{M}_{k-1}|$ with either sgn($\tilde{M}_k$) = 1 or sgn($\tilde{M}_k$) = -1 ($\forall k > 2$). However, it is simple to show that this scenario cannot occur with the gain adaptation law given by (13)-(15). Indeed, the error $\tilde{M}$ will never take more than one consecutive step in the wrong direction, i.e., will not result in $|\tilde{M}_{k+1}| > |\tilde{M}_k| > |\tilde{M}_{k-1}|$ for sgn ($\tilde{M}_{k+1}$) = sgn($\tilde{M}_k$) = sgn($\tilde{M}_{k-1}$) for any k >2. (This proof has been omitted; for details, see [3].)

Since it is impossible for the sign of the adaptation step to be incorrect for more than one consecutive step, the magnitude of the adaptation step—specifically the gain $\gamma_{\Delta M}$—must be the critical factor in determining whether the gain adaptation law is stable. Fig. 6 gives an example of a situation in which the gain $\gamma_{\Delta M}$ is large enough to cause instability of M. In this example, $\left|\tilde{M}_{k+1}\right| > \left|\tilde{M}_{k-1}\right|$, $\forall k > 2$ but $\left|\tilde{M}_{k+1}\right| \not> \left|\tilde{M}_k\right|$, $\forall k > 2$.

2. Bounds on Gain $\gamma_{\Delta M}$ for Stability

Since this type of instability can occur whenever $|\Delta M_k| > |\tilde{M}_{k-1}|$, it is logical to consider

$$|\Delta M_k| = |\tilde{M}_{k-1}|, \quad \tilde{M}_{k-1} \neq 0 \tag{22}$$

to be the critical case, which may be referred to as the marginal stability case. For the symmetrical curve

$$f(\tilde{M}_{k-1}) = f_k = a\tilde{M}_{k-1}^2 + b, \tag{23}$$

where $a < 0$ and b is any real number, the $\gamma_{\Delta M}$ that makes (22) true is simple to find.

In the critical gain scenario of this example, the system is oscillating among the three points plotted in Fig. 7. If $\Delta M_k = \tilde{M}_{k-1}$, then $\tilde{M}_k = 0$ by (13). Further, substituting f_k for P_{favg_k} in (15) and considering (14), in this case the gain $\gamma_{\Delta M}$ is such that $\Delta M_{k+1} = \Delta M_k$, so $\tilde{M}_{k+1} = -\tilde{M}_{k-1}$. Following the equations through one more step shows that $\tilde{M}_{k+2} = 0$, and the adaptive gain will oscillate among these three points. Thus, an upper bound on the gain $\gamma_{\Delta M}$ for stability can be found by equating

$$\Delta M_k = \tilde{M}_{k-1} = -\tilde{M}_{k+1} \tag{24}$$

and solving for $\gamma_{\Delta M}$ in terms of a given $\tilde{M}_k = 0$, which

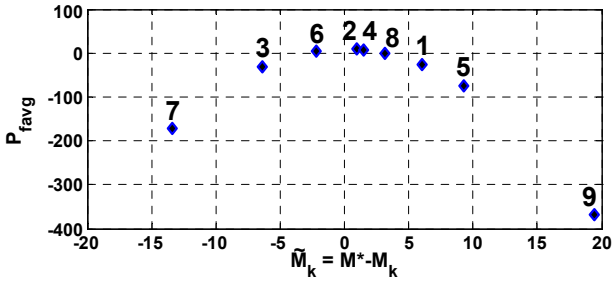

Fig. 6. Instability example for gain adaptation law. This type of instability is possible if the gain $\gamma_{\Delta M}$ in the gain adaptation algorithm is too large.

yields

$$\gamma_{\Delta M} = \pm\sqrt{\tfrac{1}{|a|}}. \tag{25}$$

Since $\gamma_{\Delta M} > 0$, the positive value of (25) is chosen. Thus, the gain adaptation law (13)-(15) will not cause instability of $\tilde{M}$ on the curve (23) whenever $0 < \gamma_{\Delta M} < |a|^{-\frac{1}{2}}$. In fact, since $\gamma_{\Delta M} = |a|^{-\frac{1}{2}}$ is the marginal stability case, $0 < \gamma_{\Delta M} < |a|^{-\frac{1}{2}}$ will actually cause convergence of $\tilde{M} \to 0$.

Since the requirement on $\gamma_{\Delta M}$ is dependent on the magnitude $|a|$, any $\gamma_{\Delta M}$ chosen for a specific curve will also guarantee convergence of M on a shallower curve—i.e., one with a smaller $|a|$. A similar result can be stated for an asymmetric curve: if the gain $\gamma_{\Delta M}$ is chosen to guarantee convergence based on the slope of the steeper side of the curve, it would guarantee convergence over the entire curve. Thus, for any turbine P_{favg} vs. $\tilde{M}$ curve, there exists a $\gamma_{\Delta M}$ that guarantees convergence of the adaptive gain M, and this $\gamma_{\Delta M}$ depends on the steepness of the P_{favg} vs. $\tilde{M}$ curve.

3. Asymmetric P_{favg} vs. $\tilde{M}$ Curves

Unfortunately, the P_{favg} vs. $\tilde{M}$ curve is not known for any turbine, so an approximation is necessary in practice. A more conservative selection of $\gamma_{\Delta M}$ is then likely to result in stability (and convergence), but will also result in smaller step sizes and may thus experience slower

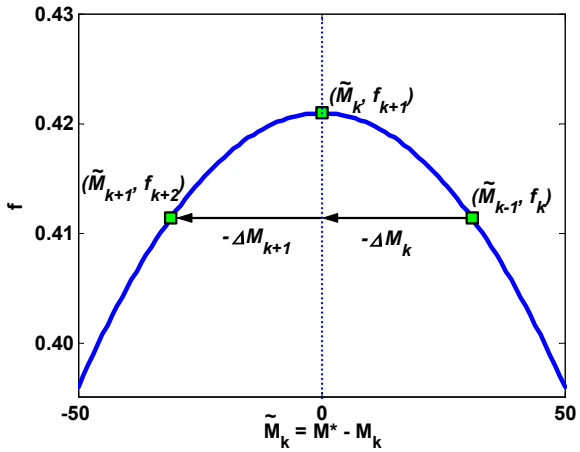

Fig. 7. Finding the critical gain.

convergence.

An example of the selection of $\gamma_{\Delta M}$ is provided in Fig. 3. The y curve is chosen to fit snugly inside the P_{favg} curve while satisfying $f < P_{favg}$; in this case, a = -0.00001. Thus, the maximum allowable $\gamma_{\Delta M}$ for stability is 316. The gain used in testing on the CART (before this stability analysis was performed) was $\gamma_{\Delta M}$ = 100, which was determined empirically from simulations and early hardware testing. Although actual turbine results indicate stable performance of the adaptive control law, this stability analysis provides further reassurance and guidelines in choosing $\gamma_{\Delta M}$.

A formal proof of the stability of the feedback system given by Fig. 4(b) with one modification is provided in the appendix. Following the proof, we present an argument as to the why the modified proof is still relevant.

V. CONCLUSION AND FUTURE WORK

We previously developed an adaptive control scheme for region 2 control of a variable speed wind turbine. In this paper, we have addressed the question of theoretical stability of the adaptive controller and have determined that the rotor speed is asymptotically stable under the basic torque control law and $\mathcal{L}_2$ stable with respect to the wind input. Further, we have devised a method for selecting $\gamma_{\Delta M}$ in the gain adaptation law to yield convergence of the adaptive gain M. Future work will include extensions such as incorporating further past values of M into the control law to reduce oscillatory behavior.

APPENDIX: THE STABILITY PROOF

The proof in this appendix, which is given in more detail in [3], is based on the sector stability criterion given by Theorem 2.2 in [12], hereafter referred to as Safonov's Theorem 2.2. This theorem applies to the two subsystem feedback system given in Fig. 8(a), where d_1 and d_2 are disturbance inputs to each subsystem. The disturbances in this proof can be considered to enter the subsystems additively, as shown in Fig. 8(b).

Safonov's Theorem 2.2 incorporates a functional F operating on the signals $x \in X_e$ and $y \in Y_e$, where X_e and Y_e are extended normed spaces. F defines an inner product on x and y as follows:

$$F(x,y,t) \equiv \langle F_{11}y + F_{12}x, F_{21}y + F_{22}x \rangle_t, \tag{26}$$

where t denotes a truncation defined by the usual truncation operator; $F_{11}0 = F_{12}0 = F_{21}0 = F_{22}0 = 0$; F_{11}, F_{21}: $Y_e \rightarrow \mathcal{L}_e$; and F_{12}, F_{22}: $X_e \rightarrow Y_e$. In this definition, $\mathcal{L}_e$ is an extended inner product space. The sector of F is defined using the inner product (26):

$$\text{sector}(F) \equiv \left\{ (x,y) \in X_e \times Y_e \,\middle|\, F(x,y,t) \le 0 \forall t \in T \right\}. \tag{27}$$

In (27), for the purposes of this analysis, T = [0,∞) is considered to be time. Now, Safonov's Theorem 2.2 requires the following:

(a) F is as given in (26) and F_{11}, F_{12}, F_{21}, and F_{22} have finite incremental gain.

(b) The mappings d_1 into $S_1(d_1)$ and d_2 into $S_2(d_2)$ are bounded about $S_1(0)$ and $S_2(0)$.

(c) $S_1^{-1}(0)$ is strictly inside sector(F) and S_2 is outside sector(F).

Safonov's Theorem 2.2 concludes that, given (a) – (c), the system depicted in Fig. 8(a) has a bounded closed-loop gain.

Now, consider the wind turbine controller with the modified gain adaptation law

$$\Delta M(k) = \gamma_{\Delta M} \operatorname{sgn}[\Delta M(k-n)] \Delta P_{favg}(k). \tag{28}$$

First, decompose the system given by (13), (15), and (28) into the block diagram in Fig. 9. The nonlinearity N_2 captures the relationship between $\tilde{M}$ and fractional mean power P_{favg}. Denote

$N_1(y) \equiv \gamma_{\Delta M} \operatorname{sgn}(y) | y | = \gamma_{\Delta M} y$, $N_3(x,\alpha) \equiv x\alpha$, $N_4(\beta) \equiv \operatorname{sgn}(\beta)$.

ΔM is the input to S_{21}. The output of S_{21} is given by $y = \overline{N}_2(\Delta M)$. Let p_* denote the minimal slope of N_2 in the domain of interest and let p^* denote its maximal slope; without loss of generality, let $p_* = -p^*$. The output of the linear block H_2 is $\tilde{M}$, and the output of the nonlinear block N_2 is P_{favg}. Further note that y, the output of S_{21}, corresponds to ΔP_{favg}. Then,

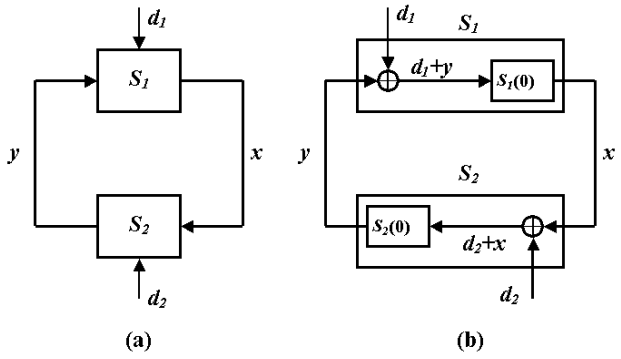

Fig. 8. Feedback systems considered by Safonov: (a) general case, and (b) specific case with disturbances entering additively.

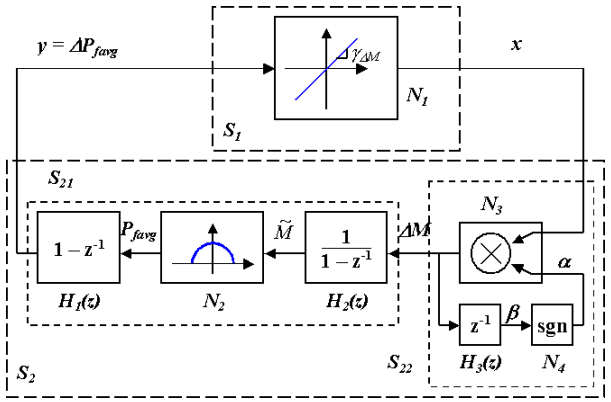

Fig. 9. Adaptive control feedback system. This system depicts a slight modification of the gain adaptation law presented in (13) – (15).

$$\Delta P_{favg_k} = y_k = \overline{N}_2(\Delta M_k) = N_2(\widetilde{M}_{k-1} - \Delta M_k) - N_2(\widetilde{M}_{k-1}). \quad (29)$$

describes the relationship between ΔM and ΔP_{favg} in the subsystem S_{21}. For any given $\widetilde{M}_{k-1}$ in the domain of interest, the relationship (29) is simply the slope of the line segment connecting the points ($\widetilde{M}_{k-1}$, $N_2(\widetilde{M}_{k-1})$) and ($\widetilde{M}_{k-1} - \Delta M_k$, $N_2(\widetilde{M}_{k-1} - \Delta M_k)$). Although the magnitude and sign of this slope for a given input ΔM_k vary depending on $\widetilde{M}_{k-1}$, the slope nevertheless is bounded by the maximal and minimal slope of the nonlinearity N_2 as long as these points are within the domain of interest. Note that when $\Delta M_k \in \mathcal{L}_{\infty e}$, so is $\widetilde{M}_k$ since the gain of H_2 is bounded when operating on an extended normed space.

Now, let x be the input to the subsystem S_{22}, or equivalently the input to S_2. Then, $\Delta M_k = (x_k)(\mathrm{sgn}(\Delta M_{k-1}))$ and

$$y_k = N_2(-x_k \,\mathrm{sgn}(\Delta M_{k-1}) - \sigma_k) - N_2(-\sigma_k), \quad (30)$$

where $\sigma_k = \sum_{i=1}^{k-1} x_i \,\mathrm{sgn}(\Delta M_{i-1})$. Note that (30) is similar in nature to (29). In order to use Safonov's Theorem 2.2 to examine stability of this system, we must first select an appropriate sector functional F. In this case, let X_e and Y_e be the extended normed space $\mathcal{L}_{\infty e}$ and let the components of F be $F_{11} = F_{21} = 1$, $F_{12} = p^*$, and $F_{22} = -p^*$. Since p^* is bounded, requirement (a) is satisfied. Similarly, since the disturbance inputs are additive as shown in Fig. 8(b), the requirement (b) is automatically satisfied. Now, only requirement (c) remains to be shown.

Define the inner product in the usual way for discrete time systems, i.e., $\langle x, y \rangle_t = \sum_{i=1}^{t-1} x_i y_i$. Then, the operator F gives the following inner product for this system:

$$\langle y + p^* x, y - p^* x \rangle_t = \sum_{k=1}^{t-1} \left\{ \left[N_2(-x_k \,\mathrm{sgn}(\Delta M_{k-1}) - \sigma_k) - N_2(-\sigma_k) \right]^2 - (p^* x_k)^2 \right\} \quad (31)$$

Now, given the maximal and minimal slope of the nonlinearity N_2, we know that

$$\left| N_2(-x_k \,\mathrm{sgn}(\Delta M_{k-1}) - \sigma_k) - N_2(-\sigma_k) \right| < p^* |x_k|,$$

where $|x_k|$ can replace $-x_k \mathrm{sgn}(\Delta M_{k-1})$ for simplicity because the slope of the line segment connecting the two points is bounded by the same value (p^*) regardless of whether the input x is positive or negative. Thus, the sum given by (31) is less than or equal to zero for all t. This result proves that the graph of subsystem S_2 lies inside the sector($[-p^*, p^*]$). To use the notation in Safonov's Theorem 2.2, let sector(F) be the *complement* of sector($[-p^*, p^*]$), i.e., sector(F) = sector($[p^*, -p^*]$). Then, the graph of S_2 lies *outside* the sector(F). Also, the subsystem S_1 is a positive memoryless linear operator with gain $\gamma_{\Delta M}$ whose graph is simply a line through the origin having slope equal to $\gamma_{\Delta M}$. Thus, the graph of the inverse of S_1 is a line through the origin having slope equal to $1/\gamma_{\Delta M}$. Requirement (c) of Safonov's Theorem 2.2 is satisfied if this line with slope $1/\gamma_{\Delta M}$ lies *strictly inside* the sector(F). Thus, $\gamma_{\Delta M}$ must be chosen such that $\gamma_{\Delta M} < 1/p^*$; if this inequality holds, then the system given in Fig. 9 has a bounded closed-loop gain.

Remark: A stable system may still be obtained by replacing the term $|\Delta P_{favg}(k)|$ with the more aggressive term $|\Delta P_{favg}(k)|^{1/2}$. Note that, with such an update, the subsystem S_1 is no longer a memoryless linear operator with gain $\gamma_{\Delta M}$ but rather a memoryless monotonically increasing positive nonlinearity with graph bounded by the sector($[0,\infty)$). If it can be shown that the magnitude of the open-loop gain is less than unity, stability of the system is established by Theorem 1 in [13]; equivalently, the circle criterion and related multiplier theory techniques can also be used to establish the stability. Future work will include a rigorous proof, but, roughly speaking, the proof will show that the gain of S_2 is arbitrarily small around the operating point $(\Delta P_{favg}, \Delta M) = (0,0)$ since the gain of S_1 is arbitrarily large in its neighborhood. The gain of S_2 may be allowed to be relatively high in the region where $|\Delta P_{favg}|$ is large since the gain of S_1 is very small for large $|\Delta P_{favg}|$.

REFERENCES

[1] P. Gipe, *Wind Energy Comes of Age*. New York: John Wiley & Sons, Inc., 1995.

[2] K. Johnson, L. Fingersh, M. Balas, and L. Pao, "Methods for increasing region 2 power capture on a variable speed HAWT," *Proc. 23rd ASME Wind Energy Symp.*, pp. 103-113, 2004.

[3] K. Johnson, "Adaptive torque control of variable speed wind turbines," Ph. D. dissertation, Dept. Elec. Eng., Univ. of CO, Boulder, CO., 2004.

[4] J. Svensson and E. Ulen, "The control system of WTS-3 instrumentation and testing," *Proc. 4th International Symp. on Wind Energy Systems*, pp. 195-215, 1982.

[5] L. Fingersh and P. Carlin, "Results from the NREL variable-speed test bed," *Proc. 17th ASME Wind Energy Symp.*, pp. 233-237, 1998.

[6] S. Walker and R. Wilson, *Performance Analysis Program for Propeller Type Wind Turbines.* Oregon State University, Corvallis, Oregon, 1976.

[7] T. Burton, D. Sharpe, N. Jenkins, and E. Bossanyi, *Wind Energy Handbook*. New York: John Wiley & Sons, Ltd., 2001.

[8] J. Freeman and M. Balas, "An investigation of variable speed horizontal-axis wind turbines using direct model-reference adaptive control," *Proc. 18th ASME Wind Energy Symp.*, pp. 66-76, 1999.

[9] Y. Song, B. Dhinakaran, and X. Bao, "Variable speed control of wind turbines using nonlinear and adaptive algorithms," *J. Wind Eng. and Industrial Aerodynamics*, vol. 85, pp. 293-308, 2000.

[10] S. Bhowmik, R. Spée, and J. Enslin, "Performance optimization for doubly-fed wind power generation systems," *IEEE Trans. Industry Applications*, vol. 35, no. 4, pp. 949-958, 1999.

[11] H. Khalil, *Nonlinear Systems*. Third Edition. Upper Saddle River, NJ: Prentice Hall, 2002, p. 242.

[12] M. Safonov, *Stability and Robustness of Multivariable Feedback Systems.* Cambridge, MA: The MIT Press, 1980.

[13] G. Zames, "On the input-output stability of time-varying nonlinear feedback systems—Part I: Conditions derived using concepts of loop gain, conicity, and positivity," *IEEE Trans. Autom. Control*, vol. 11, no. 2, pp. 228-238, 1966.

REPORT DOCUMENTATION PAGE

Form Approved
OMB No. 0704-0188

PLEASE DO NOT RETURN YOUR FORM TO THE ABOVE ORGANIZATION.

1. REPORT DATE *(DD-MM-YYYY)*	2. REPORT TYPE	3. DATES COVERED *(From - To)*
December 2004	Conference Paper	December 14 - 17, 2004

4. TITLE AND SUBTITLE
Stability Analysis of an Adaptive Torque Controller for Variable Speed Wind Turbines: Preprint

5a. CONTRACT NUMBER
DE-AC36-99-GO10337

5b. GRANT NUMBER

5c. PROGRAM ELEMENT NUMBER

6. AUTHOR(S)
K.E. Johnson, L.Y. Pao, M.J. Balas, V. Kulkarni, and L.J. Fingersh

5d. PROJECT NUMBER
NREL/CP-500-36756

5e. TASK NUMBER
WER4.3302

5f. WORK UNIT NUMBER

7. PERFORMING ORGANIZATION NAME(S) AND ADDRESS(ES)
National Renewable Energy Laboratory
1617 Cole Blvd.
Golden, CO 80401-3393

8. PERFORMING ORGANIZATION REPORT NUMBER
NREL/CP-500-36756

9. SPONSORING/MONITORING AGENCY NAME(S) AND ADDRESS(ES)

10. SPONSOR/MONITOR'S ACRONYM(S)
NREL

11. SPONSORING/MONITORING AGENCY REPORT NUMBER

12. DISTRIBUTION AVAILABILITY STATEMENT
National Technical Information Service
U.S. Department of Commerce
5285 Port Royal Road
Springfield, VA 22161

13. SUPPLEMENTARY NOTES

14. ABSTRACT *(Maximum 200 Words)*
Variable speed wind turbines are designed to follow wind speed catiations in low winds in order to maximize aerodynamic efficiency. Unfortunately, uncertainty in the aerodynamic parameters may lead to sub-optimal power capture in variable speed turbines. Adaptive generaor torque control is one method of eliminating this sub-optimality; however, before adaptive control can become widely used in the wind industry, it must be proven to be safe. This paper analyzes the stability of an adaptive torque control law and the gain adaptation law in use on the Controls Advanced Research Turbine (CART) at the National Renewable Energy Laboratory's National Wind Technology Center.

15. SUBJECT TERMS
wind energy; wind speed; aerodynamic; CART; variable speed; wind turbine; adaptive torque controller

16. SECURITY CLASSIFICATION OF:			17. LIMITATION OF ABSTRACT	18. NUMBER OF PAGES	19a. NAME OF RESPONSIBLE PERSON
a. REPORT	b. ABSTRACT	c. THIS PAGE			19b. TELEPONE NUMBER (*Include area code*)
Unclassified	Unclassified	Unclassified	UL		

Standard Form 298 (Rev. 8/98)
Prescribed by ANSI Std. Z39.18